Polymer 51 (2010) 6268–6277

Contents lists available at ScienceDirect

Polymer

journal homepage: www.elsevier.com/locate/polymer

In situ grown fibrous composites of poly(DL-lactide) and hydroxyapatite as potential tissue engineering scaffolds

Jiangang Chen [a], Xiaohong Li [a,b,*], Wenguo Cui [a], Chengying Xie [b], Jie Zou [a], Bin Zou [b]

[a] Key Laboratory of Advanced Technologies of Materials, Ministry of Education, School of Materials Science and Engineering, Southwest Jiaotong University, Chengdu 610031, PR China
[b] School of Life Science and Engineering, Southwest Jiaotong University, Chengdu 610031, PR China

ARTICLE INFO

Article history:
Received 10 July 2010
Received in revised form
5 September 2010
Accepted 26 October 2010
Available online 31 October 2010

Keywords:
In situ grown fibrous composites
Mechanical properties
Tissue engineering scaffold

ABSTRACT

In situ grown hydroxyapatite (HA) within electrospun poly(DL-lactide) (PDLLA) fibers were initially investigated as potential tissue engineering scaffolds with respect to the mechanical performances, biomineralization capability, degradation behaviors, cell growth and differentiation profiles. The tensile strength and Young's moduli of *in situ* grown composites (IGC) were 8.2 ± 1.1 and 63.5 ± 5.6 MPa, respectively, which were significantly higher than those of blend electrospun composites (BEC) with 25.2% of HA inoculation. The interactions between HA and matrix polymers were approved by the red-shifts of C=O stretching and OH− stretching modes and the increases in glass transition temperatures of fibrous composites. The localization of apatite phase on the fiber surface improved the biomineralization capability and enhanced the morphological stability of the fibers and fibrous mats even when the degradation of matrix polymers was detected. The cell viability and alkaline phosphatase levels were significantly higher for composites IGC, indicating favorable scaffolds for cell proliferation and osteogenic differentiation.

1. Introduction

The development of ideal scaffolds for regenerating damaged tissues with full recovery of their biological functions has long been a major goal in tissue engineering. The high complexity degree of intrinsic properties of the natural tissues imposes the need to define appropriate strategies for the design and fabrication of scaffolds with tailored properties. The scaffolds should mimic the three-dimensional microporous structure and biological functions of extracellular matrix (ECM) so that cells can undergo proliferation and differentiation to specific tissue as they would have naturally. A wide variety of preparation techniques to generate porous scaffolds have been reported, such as solvent casting/particle leaching, solid free fabrication, temperature-induced phase separation, and microsphere sintering [1]. Electrospun nanofibrous scaffolds contain nanoscale fibers with microscale interconnected pores, resembling the topographic features of ECM, and possess an extremely high surface-to-volume ratio, tunable porosity, and malleability to conform over a wide variety of sizes and shapes, which resulted in suitable substrates for tissue engineering [2]. Electrospun fibrous nanocomposites of hydroxyapatite (HA) and poly(DL-lactic acid) (PDLLA) combine the osteoconductivity and bone-bonding ability of HA, and emulate the basic building blocks of those naturally mineralized collagen nanofibers, which would possess great potential for engineering functional bone-like substitutes [3].

In the past few years, some attention has been paid on the preparation of electrospun fibrous HA/PDLLA composites. Blend electrospinning of β-tertiary calcium phosphate and PDLLA matrix was investigated, and an increase in surface hydrophilicity and improvement of cell adhesion and proliferation were determined for the fibrous composite scaffold. However, homogeneous dispersion of nanoparticles within polymer matrices was difficult to attain due to the nanoparticle agglomeration, and lower contents of the ceramic component were indicated within the fibrous matrix [4]. To enhance the dispersion into the polymer solutions, HA nanoparticles were modified with a surfactant, hydroxysteric acid [5], or through grafting with low molecular weight PDLLA [6], and composite fibers were fabricated from blend electrospinning of modified HA nanoparticles and PDLLA matrix. The nanoparticles were dispersed uniformly in the fibers at lower HA contents than 4%. However, HA nanoparticles began to aggregate with the increase in HA contents. In addition, electrospinning of blends made by simply mixing the prior obtained inorganic nanoparticles

* Corresponding author. School of Materials Science and Engineering, Southwest Jiaotong University, Chengdu 610031, PR China. Tel.: +86 28 87634023; fax: +86 28 87634649.
E-mail address: xhli@swjtu.edu.cn (X. Li).

0032-3861/$ – see front matter © 2010 Elsevier Ltd. All rights reserved.
doi:10.1016/j.polymer.2010.10.050

with viscous spinning solutions of polymer carriers gave rise to problems like compromised electrospinnability, and reduced nanoparticles loading capacity.

The mechanical performances, subsequent cellular growth and tissue development depend in part on the characteristics of the scaffold. Scaffolds which are intended for tissue regeneration purposes need to be robust enough for both handling and sterilization, and to exhibit mechanically supportive properties for cellular morphogenesis. The strength of fibrous mats depends both on the physical properties of nanofibers such as diameter, pore size, and porosity, and on chemical properties such as the composition and crystallinity of the fiber matrix [7]. The strength of fibrous composites can also be significantly improved through the homogeneous distribution of HA particles [5]. However, blend electrospinning usually resulted in nanocomposites with very limited or lacking of specific interactions between the organic and inorganic phases, and agglomeration of nanoparticles within fiber matrices. Venugopal et al. showed that the tensile strength and elastic moduli of blended fibrous mats of poly(ε-caprolactone) (PCL) and HA were no better than those of PCL nanofibers [8]. Additional limitations of blended HA/PDLLA fibrous composites involved the limited outer presentation of HA on the fiber surface, thereby decreasing the chance for osteogenic cells to contact with the bioactive HA and resulting in weak bioactivities, such as the biomineralization capability, and unfavorable cellular responsiveness.

Attempts have been made to achieve formation of HA on PDLLA fibers after alkaline treatment [9], grafting with gelatin [10], and modifying with different chemical groups [11]. The processing parameters and formation mechanism of HA/PDLLA composites were thoroughly investigated. We previously applied electrospun nanofibers as the reaction confinement for composite fabrication. PDLLA ultrafine fibers with calcium nitrate entrapment were prepared by electrospinning, and then incubated in phosphate solution to form *in situ* calcium phosphate on the fiber matrix. The formation of non-stoichiometric nanostructured HA and well dispersion of HA particles on the electrospun fibers were obtained [12]. In the current study, fibrous HA/PDLLA composites were formed from *in situ* growth of HA within ultrafine fibers with different HA inoculations. A deep insight into the interactions between HA and PDLLA matrix were initially investigated to clarify the enhancement of mechanical performance. The biomineralization capability, degradation profiles and cell growth behaviors were initially determined on *in situ* grown HA/PDLLA composites as potential tissue engineering scaffolds, with comparison to the blended HA/PDLLA fibrous scaffolds.

2. Experimental section

2.1. Materials

PDLLA ($M_w = 147$ kDa, $M_w/M_n = 1.33$) was synthesized prepared by bulk ring-opening polymerization of DL-lactide using stannous chloride as initiator [13]. The molecular weight was determined by gel permeation chromatography (GPC, Waters 2695 and 2414, Waters Inc., Milford, MA) with a Styragel HT 4 column (7.8 × 300 mm) using polystyrene beads as standard. The mobile phase consisted of tetrahydrofuran (THF, Thermo Fisher Scientific Inc., Fair Lawn, NJ) using a regularity elution at a flowing rate of 1.0 ml/min. Ultra-pure water from a Milli-Q biocel purification system (UPI-IV-20, Shanghai UP Scientific Instrument Co., Shanghai, China) was used. All other chemicals and solvents were of reagent grade or better and purchased from Changzheng Regents Co. (Chengdu, China) unless otherwise indicated.

2.2. Preparation of HA/PDLLA fibrous composites

The fibrous composite of *in situ* growth of HA within electrospun PDLLA fibers (IGC) was prepared as described elsewhere [12]. Briefly, calcium nitrate and PDLLA were dissolved in THF, and the mixed solution was added in a 5 ml syringe attached with a circular-shaped metal syringe needle as the nozzle. The flow rate was controlled within 3.6 ml/h by a precision pump (Zhejiang University Medical Instrument Co., Hangzhou, China) to maintain a steady flow from the capillary outlet. The electrospinning voltage was set at 20 kV, and the grounded collector was located about 150 mm apart from the capillary tip. The fiber collections were vacuum dried at room temperature for 3 d to remove remaining organic solvent prior to further use [14]. The electrospun non-woven fibrous mats with calcium salts entrapment were sectioned into 80 × 80 mm^2 with the thickness of 0.5 mm and soaked in pH 9.0 diammonium phosphate solution at 25 °C for 7 d. After gently rinsed with pure water, the fibrous composite was dried as above. The composite IGC was dissolved into THF, and the suspension was electrospun as above to prepare the blended HA/PDLLA fibrous composite (BEC). HA was removed from the above suspension by centrifugation, and the resulting polymer solution was electrospun into ultrafine PDLLA fibers as control.

2.3. Characterization of fibrous composites

2.3.1. Morphology of fibrous composites

The morphology of the HA/PDLLA fibrous composites were examined by a scanning electron microscope (SEM, FEI Quanta200, FEI Ltd, Eindhoven, The Netherlands) equipped with field-emission gun (accelerating voltage of 10 kV) and Robinson detector after 2 min of gold coating to minimize charging effect. The fibers diameter was measured from SEM images with the magnification of 10,000, and five images were used for each fibrous sample. From each image, at least 20 different fibers and 200 different segments were randomly selected and their diameter measured to generate an average size by using the tool of Photoshop 10.0 edition [15]. The semi quantitative elemental analysis of the formed HA on the fibrous composites was carried out by an energy dispersive X-ray analyzer (EDX) attached to SEM operated at 20 kV. Three runs were made on different spots on each specimen.

2.3.2. Characterization of HA in fibrous composites

The distribution patterns of HA particles in the fibrous composites were characterized by a transmission electron microscope (TEM, Hitachi H-700H, Hitachi Co. Ltd., Japan). TEM was operated at 15 kV, and the fiber samples were prepared by directly depositing the as-spun ultrafine fibers onto copper grids. The composite IGC was dissolved into THF, and HA was collected from the above suspension by centrifugation. The dispersion morphologies of HA powders were observed by TEM as indicated above.

To investigate the crystalline phase of calcium phosphate formed on PDLLA fibers, fibrous composites were analyzed using X-ray powder diffraction (XRD, Philips X'Pert PRO, Philips, The Netherlands) employing Cu *Ka* radiation (30 kV, 10 mA). The diffraction patterns were collected with 2θ ranging from 20° to 60° with a scanning speed of 0.35°/min.

2.3.3. Surface wettability of fibrous composites

Surface wettability of the various substrates was characterized by measuring the water contact angle (WCA) at room temperature. A drop of purified water was deposited onto the mat surface using a micro-syringe attached on the goniometer (DSA 100 Mk 2, Krüss GmbH, Hamburg, Germany), followed by image processing of the sessile drop with DSA 1.8 software. At least 6 droplets were tested on different parts of each mat.

2.3.4. Mechanical properties of fibrous composites

The fibrous composites were punched into small strips ($70.0 \times 7.0 \times 0.6$ mm^3), and the uniaxial tensile properties were characterized on dry samples using a mechanical testing machine (Instron 5567, Instron Corp., Canton, MA). The stress–strain curves of the fibrous mats were constructed from the load deformation curves recorded at a stretching speed of 0.5 mm/s. Four separate runs were performed for each sample, and Young's modulus, tensile strength, and elongation at break were obtained from the stress–strain curves.

2.4. Characterization of HA interactions with matrix polymers

The composite formation and the interactions of HA with the fiber matrix were investigated by Fourier transform infrared spectrometer (FTIR, Thermo Nicolet 5700, Thermo Nicolet Instrument Corp., Madison, WI). The spectra were collected over the range of 4000-400 cm^{-1} using KBr pellets, and the transmittance between 2000 and 1500 cm^{-1} was recorded with 4 scans with resolution of 1 cm^{-1} adopted to characterize various functional groups [16].

To qualitatively determine the amount of HA and the glass transition temperature of PDLLA in the fibrous composites, thermogravimetric analysis (TGA) and differential scanning calorimetry (DSC) were tested (Netzsch STA 449C, Netzsch, Bavaria, Germany). Approximately 10 mg of each sample was loaded within the measurement chamber and the scanning range was from room temperature to 500 °C with an ascending rate of 5 °C/min in perforated and covered aluminum pans under a nitrogen purge.

2.5. Biomineralization behaviors of fibrous composites

The biomineralization capability can be evaluated *in vitro* by monitoring the formation of apatite when immersed in simulated body fluids (SBF) whose ionic composition emulates blood plasma closely [17]. Briefly, the fibrous mats were sectioned into 80×80 mm^2 with the thickness of 0.5 mm. Each specimen was immersed in 1.5× SBF at 37 °C for 7 d, which was maintained using the thermostated water bath (Taichang Medical Apparatus Co, Jiangsu, China). The suspensions were changed with fresh SBF every other day. Upon removal from SBF at predetermined intervals, the fibrous mats were gently rinsed with pure water and dried as above. The morphologies of mineralized fibrous mats were observed by SEM. The mineralized mass and crystallinity were measured by TGA and XRD, respectively. The diffraction peak broadening due to small crystallites can be semi-quantitatively estimated from the Scherrer equation: $\beta_{1/2} = (K\lambda)/(D \cos \theta)$ [18], where $\beta_{1/2}$ is the full-width at half maximum in 2 h calculated by the XRD equipment software, K is a constant set to 1, λ is the X-ray wavelength in Angstroms, D roughly indicates the average crystallite size, and θ is the diffraction angle of the corresponding reflex.

2.6. Degradation behaviors of fibrous composites

The degradation behaviors were estimated from the morphological change, molecular weight reduction and mass loss of fibrous composites. Briefly, pre-weighted fibrous mats of electrospun PDLLA fibers, composites IGC and BEC (about 150 mg each) were incubated at 37 °C in 20.0 ml of pH 7.4, 154 mM phosphate buffered saline (PBS) containing 0.02% sodium azide as a bacteriostatic agent. At predetermined intervals triplicate samples for each sample were recovered, rinsed with pure water to remove residual buffer salts, and dried to constant weight in a vacuum desiccator. The mass loss of these composite mats was caused by the hydrolytic degradation of PDLLA and the fall-off of HA nanoparticles from the fibers. Triple samples of each composite residue were dissolved into THF and centrifuged to remove inorganic salts. The mass loss of matrix polymer was determined gravimetrically by comparing the dry weight remaining at a specific time with the initial weight. The molecular weight of recovered matrix polymer was determined using GPC as described above.

2.7. Cell culture on fibrous composites

Each of fibrous mats of 250–300 μm thickness was cut into small disks (11 mm in diameter), and sterilized by ^{60}Co γ-ray at a dosage of 10 kGy. Prior to cell seeding, each sample was placed in an individual well of a 48-well tissue culture plate (TCP, Costar, Corning, NY), and soaked with cell culture medium for 12 h. The immortal pre-osteoblastic murine calvaria cell line MC3T3-E1 (CRL-2593, American Type Culture Collection, Rockville, MD) was used in this study, and maintained in α-MEM (Gibco BRL, Rockville, MD) that was supplemented with 10% fetal bovine serum (FBS, Gibco Invitrogen, Grand Island, NY) and 1% penicillin-streptomycin (Sigma–Aldrich Inc., St. Louis, MO). A total of 100 μl cell suspension with the density of 8×10^3 cells/ml was carefully seeded onto the surface of each fibrous disk. The cell-seeded scaffolds were incubated at 37 °C in a humidified atmosphere for 2 h to make cells diffuse into and adhere onto the scaffold before the addition of 1.0 ml of culture medium into each well. The cell-seeded scaffolds were replenished with fresh media every 2 d.

2.8. Cell viability, differentiation and morphology analyses

Cell viability was assayed by Cell Counting Kit-8 reagent (CCK-8, Dojindo Laboratories, Kumamoto, Japan). The mechanism behind this assay is that, metabolically active cells react with tetrazolium salt in CCK-8 reagent to produce a soluble formosan dye that can be observed at 450 nm. Briefly, on days 3, 5, and 7 after incubation, cell grown fibrous mats were transferred to another 48-well TCP filled with 400 μl of fresh RPMI1640 (Gibco BRL, Rockville, MD) with 10% FBS in each well. After incubation at 37 °C for 1 h, 40 μl of CCK-8 reagent was added into each well and incubated for 4 h according to the reagent instruction. An aliquots (150 μl) of incubated medium were pipetted into 96-well TCP and read in a spectrophotometric plate reader at 450 nm (Elx-800, Bio-Tek Instrument Inc., Winooski, VT).

The differentiation of precursor cells to osteoblasts was determined by measuring their alkaline phosphatase (ALP) activity [19]. Briefly, after 3, 5 and 7 d culture, the media were removed and the cell grown fibrous mats were washed twice with PBS. Then 100 μl/well of 0.1% Triton X-100 (Amresco Inc., Solon, OH) was used to lyse the cells for 5 min at room temperature. The chromogenic substrate for ALP was 10 mM 4-nitrophenyl phosphate (F. Hoffmann-La Roche AG, Basel, Switzerland) dissolved in water with 0.5 M tris-base (Amresco Inc., Solon, OH) for 60 min. Then, the ALP concentration was determined by kinetic measurement of the absorbance at 405 nm in a spectrophotometric plate reader. The result was normalized to the control of untreated cells and presented as the relative total ALP activity.

The morphologies of cells grown on fibrous mats were observed by SEM. Briefly, fibrous mats were washed with PBS twice, and then fixed in 2.5% glutaraldehyde for 6 h at 4 °C. Following three rinses with distilled water, the samples were dehydrated through a series of graded ethanol solutions and then freeze-dried. Dry constructs were sputter coated with gold and observes by SEM at an accelerating voltage of 20 kV.

2.9. Statistics analysis

The values were expressed as means ± standard deviation (SD). Whenever appropriate, two-tailed Student's *t*-test was used to

discern the statistical difference between groups. A probability value (p) of less than 0.05 was considered to be statistically significant.

3. Results and discussion

Blend Electrospinning of HA and polymer solutions gave rise to problems like compromised electrospinnability, and reduced nanoparticles loading capacity. The weak molecular interaction between HA and matrix polymers and poor dispersion of HA into fiber matrices resulted in the deterioration of mechanical properties. *In situ* growth of HA was introduced to use electrospun nanofibers as reaction confinement for the fabrication of HA/PDLLA fibrous composites. To achieve a better application of the fibrous composites in biomedical fields, the mechanical properties, biomineralization capability, degradation behavior, and cell growth and differentiation profiles were evaluated in this study.

3.1. Characterization of HA/PDLLA fibrous composites

Fig. 1 shows SEM images of electrospun fibrous mats, fibrous composites BEC and IGC. The electrospun fibrous mats were porous with bead-free and randomly arrayed fibers (Fig. 1a). The calcium-loaded polymer fibers were incubated with phosphate solution, and calcium phosphates were formed by precipitation reaction with calcium ions entrapped within fibers. Fig. 1c shows the distribution morphology of calcium phosphate particles on the fiber matrix of the composite IGC. It was difficult to estimate the exact size of HA crystals from SEM images, but it did appear that the *in situ* formation of HA was made up of very ultrafine particles that were homogeneously distributed on the fiber surface. The inset of Fig. 1c shows the TEM profile of the composite IGC, indicating the dispersion of HA nanoparticles along the fiber surface. Compared with the rough surface of the composite IGC, the composite BEC

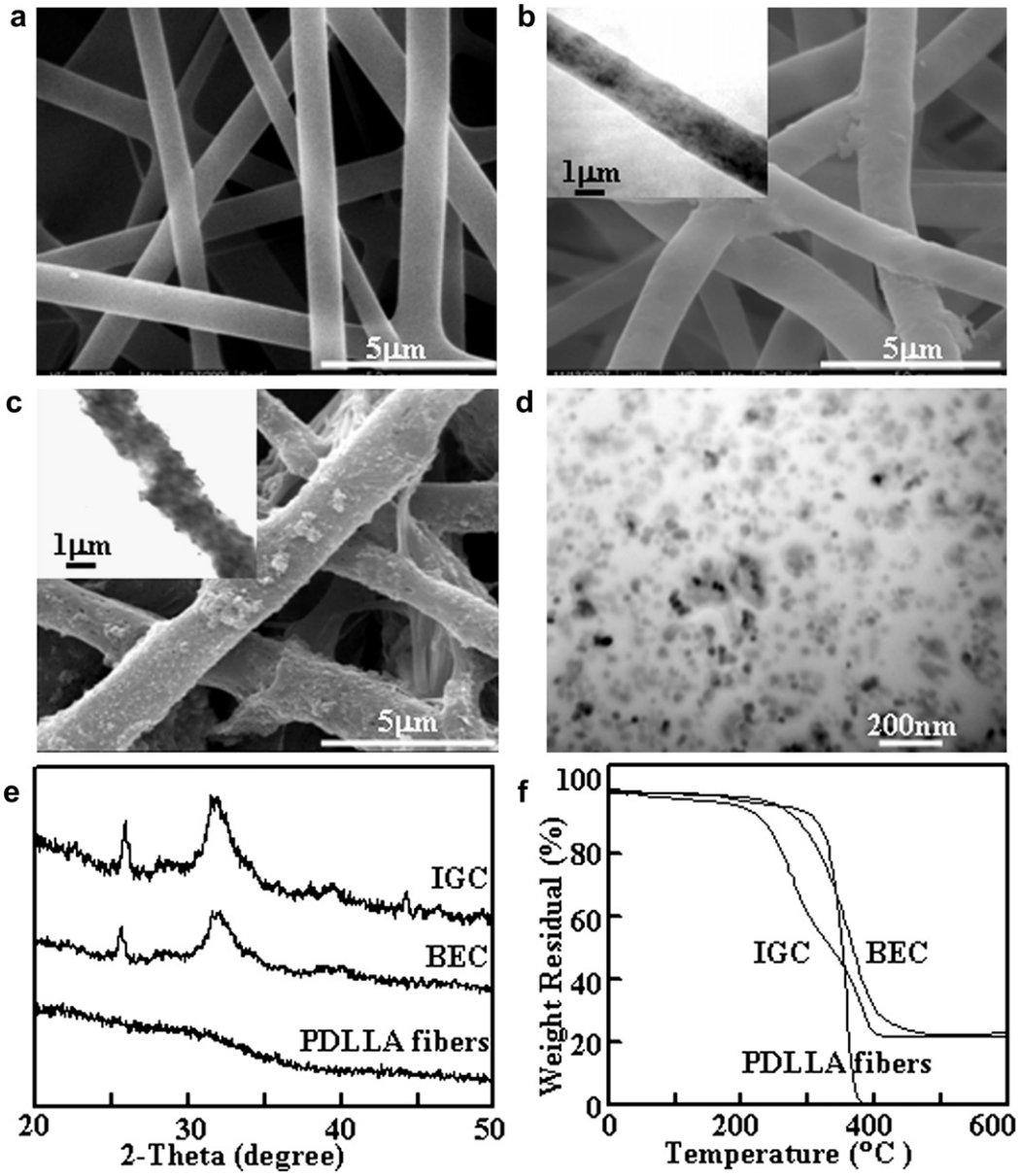

Fig. 1. SEM images of electrospun PDLLA mats (a), HA/PDLLA fibrous composites from blend electrospinning (BEC, b) and *in situ* growth (IGC, c), and insets show TEM profiles; (d) TEM image of HA nanoparticles collected from the suspension after dissolving of composites IGC into THF; XRD patterns (e) and TGA curves (f) of electrospun PDLLA fibers, composites IGC and BEC with 25.2% of HA loadings.

was smooth and uniform, and HA nanoparticles homogeneously distributed within the fibers (Fig. 1b). The electrospinning parameters were optimized, and electrospun PDLLA mats, fibrous composites IGC and BEC indicated close fiber diameters of 786 ± 203, 843 ± 107 and 905 ± 140 nm, and the porosity was 79.2 ± 2.4%, 75.4 ± 1.6% and 72.6 ± 2.2%, respectively. The composites were dissolved in THF and HA particles were extracted through centrifugation. Fig. 1d shows the TEM image of HA nanoparticles extracted from the composite IGC. Although there were some particle agglomerations, the size of HA nanoparticles ranged from 40 to 60 nm.

XRD patterns of electrospun PDLLA fibers and the formed composites are shown in Fig. 1e. A big broad peak centered at $2\theta = 31.8^\circ$, a broad peak at $2\theta = 25.8^\circ$ and smaller broad peaks at $2\theta = 28^\circ$, 42° and 47° were shown in the XRD profiles of composites IGC and BEC, which are characteristic patterns of HA [20]. The broad peaks were seemingly designated as non-stoichiometric HA and low-crystalline apatitic phase, which may be a mixture of amorphous calcium phosphate (ACP) and crystalline HA. There were also other forms of crystalline calcium phosphate phases, such as octacalcium phosphate (OCP) [21], as seen from XRD patterns of the composites. The average Ca/P ratio was 1.65, measured from EDX pattern of the mineralized fibrous mat. As shown in Fig. 1e, the strength of peaks indicated that slightly higher crystallinity of HA was formed in the composite IGC than that of BEC. It was indicated that the electrospinning process had some effects on the HA crystallinity. TGA analysis showed that electrospun fibers lost nearly all the weight with the temperature increasing up to about 350 °C, and there were about 25.2% of calcium phosphates formed in the fibrous composites (Fig. 1f).

3.2. The mechanical properties of fibrous composites

Good evidence showed that HA nanoparticles significantly enhanced the mechanical strength of HA/polymer composites. But the improvement in mechanical properties of fibrous composites was found to be less significant. Venugopal et al. investigated composite fibers by blend electrospinning of HA and PCL matrix [8]. The tensile strengths of 3.37 and 1.07 MPa and the elastic moduli of 10.82 and 3.52 MPa were obtained for PCL and HA/PCL nanofibers, respectively. It is suspected that the distribution of HA could impinge upon the mechanical properties tested. Xu et al. modified HA nanoparticles through grafting with low molecular weight PDLLA, and composite fibers were fabricated from blend electrospinning of the modified HA nanoparticles and PDLLA matrix [6]. Almost all the composite mats electrospun from modified HA showed higher tensile strengths and moduli. The maximal strength of about 3.3 MPa was located at the HA content of 4%. TEM analysis indicated that HA nanoparticles began to aggregate with the increase in the HA contents, which resulted in the deterioration of mechanical properties. The problems of agglomeration and low HA loadings played great roles in the mechanical properties of fibrous composites.

Fig. 2a shows the stress–strain curves of electrospun PDLLA fibers, composites BEC and IGC with 25.2% of HA loadings. PDLLA ultrafine fibers with different entrapment amounts of calcium nitrate were used, and composites with 5.2%, 12.5%, 20.4% and 25.2% of HA inoculations were obtained to determine the effect of HA contents on the mechanical properties. The tensile strength, Young's moduli and elongation at break are summarized in Fig. 2b, c, and d, respectively. Composites IGC showed higher tensile strength, elongation at break and Young's moduli than composites BEC at every HA loading. As shown in Fig. 2b and c, the tensile strength and Young's moduli of composites IGC increased monotonically with the increase in HA contents. The tensile strength of composites IGC increased from 5.8 ± 1.2 to 8.2 ± 1.1 MPa, and Young's moduli from 54.2 ± 4.6 to 63.5 ± 5.6 MPa when the HA loadings increased from 5.2% to 25.2%. The elongation at break of all the composites decreased with the increase in HA loadings (Fig. 2d).

The inoculation of HA crystals with a high surface/volume ratio should offer a significant contribution to the mechanical response of the scaffold, due to the large surface area available physically to interact with the matrix. However, the agglomeration of HA

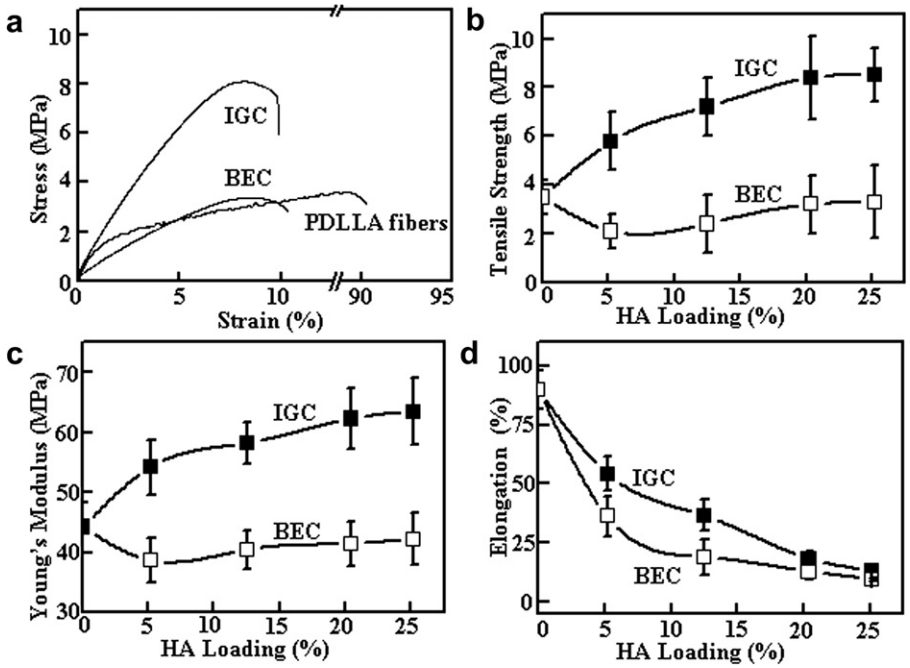

Fig. 2. The stress–strain curves (a) of electrospun PDLLA fibers, HA/PDLLA fibrous composites from blend electrospinning (BEC) and *in situ* growth (IGC) with 25.2% of HA loadings; The tensile strength (b), Young's moduli (c) and elongation at break (d) of composites BEC and IGC with different HA inoculations ($n = 4$).

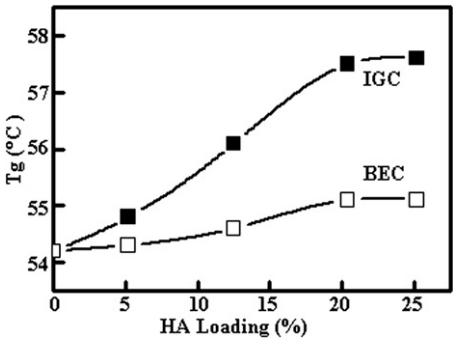

Fig. 3. Glass transition temperatures (Tg) of HA/PDLLA fibrous composites from blend electrospinning (BEC) and *in situ* growth (IGC) with different HA inoculations.

nanoparticles formed defect phases in the matrix and resulted in less integrity of the fiber structure in the composite BEC, which depleted the strengthening effect of the inorganic phase in polymer matrices. As shown in Fig. 2, there were no significant variation of the tensile strength and Young's moduli of composites BEC with different HA inoculations ($p > 0.05$). In the composites IGC, the improvement of mechanic properties could be attributed to the presence and uniform distribution of HA on the fiber surface, which protected the integrity of fiber matrix. Moreover, *in situ* growth process may enhance the interfacial interactions between the formed HA and the matrix polymer. As shown in Fig. 2, Young's moduli and tensile strength indicated no significant difference for composites IGC with high HA loadings of 20.4% and 25.2% ($p > 0.05$), which would mostly suggest that the strengthening effect of the formed HA had reached a saturation situation.

3.3. Interactions between HA and PDLLA of fibrous composites

The mechanical properties of particulate composites depend strongly on the particle size, particle loading and the stress transfer between the particles and matrix [22]. Composites BEC and IGC possessed the same particle size and particle loading in the current study, and as indicated in Section 3.1, the fiber diameter and pore size of the fibrous mats indicated no significant difference ($p > 0.05$). As mentioned above, the mechanical enhancement of *in situ* grown HA on electrospun PDLLA fibers may be attributed to interfacial bonding strength between the ceramic phase and the matrix polymer. However, the interaction mechanism between polymer and inorganic particles in composites was rarely explored [1]. During the IGC formation, calcium salts were electrospun into PDLLA fiber, followed by incubation with phosphates solution for *in situ* formation of HA within fibers. It was supposed that the calcium ions and the formed HA interact with functional groups of matrix polymers. So the interactions between HA particles and fibrous PDLLA matrices were determined in the current study through DSC and FTIR analyses to clarify the reinforcement effect as indicated above.

Fig. 3 shows the glass transition temperatures (Tg) of electrospun PDLLA fibers, HA/PDLLA fibrous composites BEC and IGC with different HA contents. A lower Tg was observed for electrospun PDLLA mats (54.2 °C) than that of native polymer (58.3 °C), which due to the inner stress and the high degree of alignment and orientation of polymer chains caused by the electrospinning process [15]. The Tg of PDLLA matrix increased when HA was included into electrospun fibers, which might be due to the adsorption of polymer chains onto HA particles, thereby restricting the movement of polymer chains. The existence of interfacial interactions between HA and matrix polymers were responsible for the increase in Tg [23]. As shown in Fig. 3, more significant increases in Tg were detected for composites IGC than that of BEC at all the HA inoculations tested, indicating stronger interactions between the polymer matrices and the formed HA in composites IGC. The interactions between HA and matrix polymers should be dissociated after dissolving of the matrix polymer, re-dispersing of HA in the polymer solution through ultrasonication, and electrospinning above suspension to obtain composites BEC.

FTIR spectra of composites BEC and IGC with 25.2% of HA loadings and electrospun PDLLA fibers are shown in Fig. 4A. It can be observed that there was a strong absorption band at 1755.1 cm^{-1} corresponding to the carbonyl group (C═O), which took a red-shift for the composite IGC compared to electrospun PDLLA fibers [24]. The bands at around 3570 cm^{-1} were ascribed to the OH− stretching mode in crystal lattice of HA. As shown in Fig. 4B, absorption peaks at 3570.6, 3570.3, 3570.0 and 3569.6 cm^{-1} were found for composites IGC with HA loadings of 5.2%, 12.5%, 20.4% and 25.2%, respectively. Fig. 4C shows the C═O stretching of composites IGC with different HA inoculations. Absorption peaks at 1754.6, 1753.3, 1751.0 and 1749.6 cm^{-1} were observed for composites IGC with HA loadings of 5.2%, 12.5%, 20.4% and 25.2%, respectively, indicating more dramatic red-shifts with the increase in HA loadings. But the red-shifts of OH− stretching and the carbonyl group

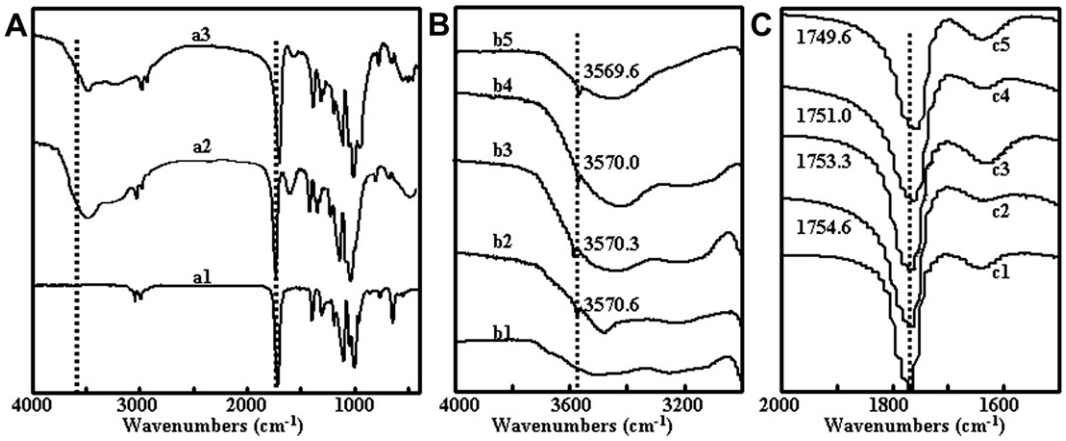

Fig. 4. (A) FTIR spectra of electrospun PDLLA fibers (a1), HA/PDLLA composites from blend electrospinning (a2) and *in situ* growth (IGC, a3) with 25.2% of HA loadings; The OH- stretching (B) and C═O stretching modes (C) in FTIR spectra of composites IGC with HA loadings of 0 (b1 and c1), 5.2% (b2 and c2), 15.2% (b3 and c3), 20.4% (b4 and c4) and 25.2% (b5and c5).

(C=O) stretching modes were not detected in composites BEC. It was possible that hydrogen bonding existed in IGC by the bonding connection of the surface P–OH of HA and C=O group of PDLLA. The bonding would be effectively transferred stress from polymer fibers to HA particles and make the reinforcement effect of composites IGC more desirable compared with that of BEC.

3.4. Biomineralization profiles of fibrous composites

In the current study, composites BEC and IGC with 25.2% of HA loadings and electrospun PDLLA fibers were examined after 7 d of immersion in SBF. Fig. 5a indicated that there was no calcium phosphate precipitate formed on electrospun PDLLA fibers during the incubation, due to the lack of bioactivity of PDLLA to induce nucleation and growth of calcium phosphate [25]. As shown in Fig. 5b and c, randomly and finely dispersed crystals were formed on the surface of composites BEC and IGC after 7 d incubation. A slight increase in the fiber size can be found in comparison with those shown in Fig. 1, due to the deposition of calcium phosphate on the fiber surface. Fig. 5d shows a homogeneous distribution of calcium phosphate particles on the fiber matrix at a higher magnification.

The XRD patterns of composites BEC and IGC and electrospun PDLLA fibers after immersion in SBF are illustrated in Fig. 5e. Sharp peaks at approximately $2\theta = 25.8^\circ$ and 31.8° were found corresponding to the main crystalline HA peaks, indicating the possible formation of HA on the fiber surface of composites IGC and BEC. Compared the XRD behaviors of composites IGC and BEC (Fig. 1e), the crystalline of the composites were enhanced after immersion in SBF. As shown in Fig. 5e, composites IGC led to a systematic sharpening in the diffraction pattern compared to composites BEC, and better crystallinity may be a result of the location of calcium phosphate precipitates on the fiber surface of composites IGC. For quantitative purposes, the line broadening of the (0 0 2) reflection range from 25° to 27° was used to evaluate the mean crystallite size, due to the fact that this peak was well resolved and showed no interference. In addition, the crystal size (0 0 2) values were related to the crystal size in the wide dimension of HA crystallites [26]. The crystal size of HA was calculated by Scherer's formula, and they were 28.6 and 42.4 nm for the composites IGC and BEC, respectively, which were similar to the apatite crystals found in bone.

TG analyses were conducted to check the amount of HA after remineralization. As indicated in Fig. 5f, the amount of HA increased from 25.2% to 48.6% and 30.2%, respectively, for composites IGC and BEC after incubation into SBF for 7 d. The surface biomineralization of the bone mineral-like Ca–P is a precondition of bioactivity as osteoconductive surface [27]. Such a type of calcium phosphate layer was bioactive when used in bone defects, and composites IGC held great potential for the mineralization of osteoblasts in bone tissue engineering. Therefore, *in situ* growth of HA particles on the fiber surface avoided randomly distribution and deterioration of

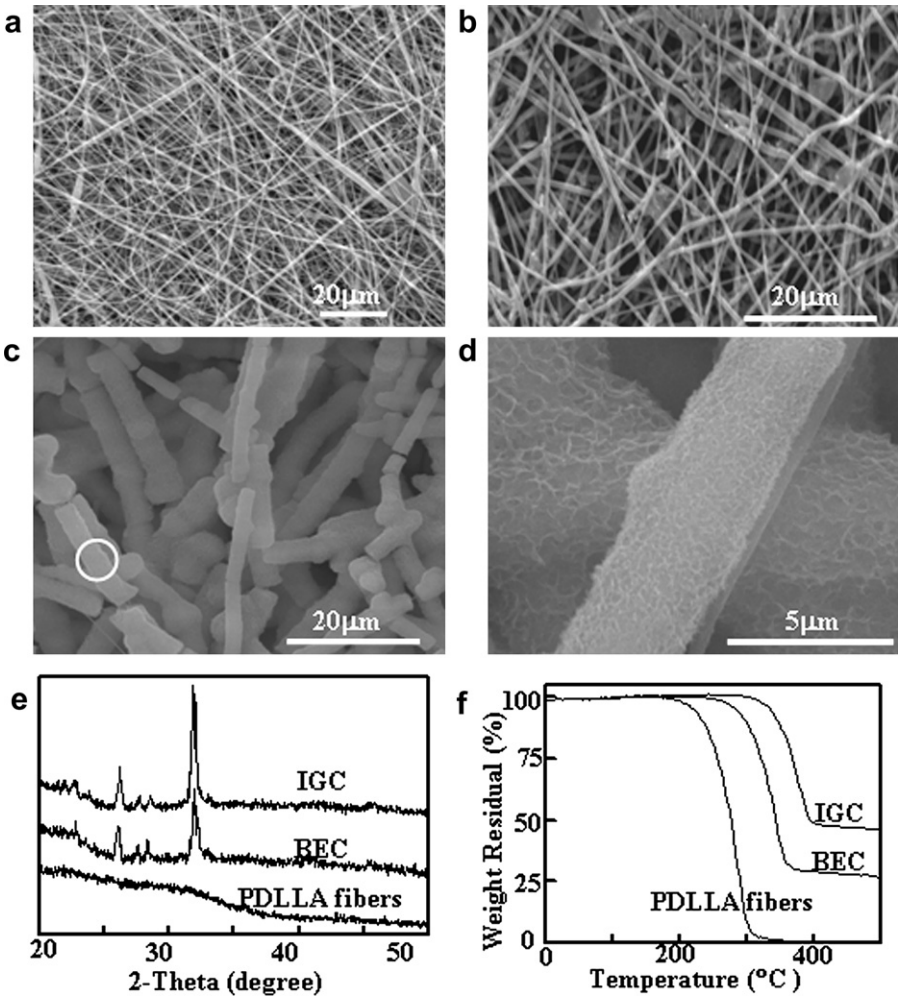

Fig. 5. SEM images of mineralized electrospun PDLLA fibers (a), HA/PDLLA fibrous composites from blend electrospinning (BEC, b) and *in situ* growth (IGC, c and d) with 25.2% of HA loadings after incubation in SBF for 7 d; XRD patterns (e) and TGA curves (f) of mineralized electrospun PDLLA fibers, composites IGC and BEC after incubation in SBF for 7 d.

the integrity of the fibrous structure, which not only enhanced mechanical performances and stable interfaces, but also obtained desirable biomineralization capability.

3.5. In vitro degradation profiles of fibrous composites

Degradation behaviors of porous scaffolds play an important role in the engineering of new tissues, since the degradation rate is intrinsically linked to cell vitality, growth as well as host response [28]. The degradation of electrospun fibers could be modulated by physically and chemically modifying the surface wettability and compositions of the fiber matrix. In the current study, the degradation of fibrous composites was determined with regard to the morphological changes of fibers, the mass loss of fibrous matrices and the molecular weight reduction of matrix polymers. Both the dissolution of PDLLA degradation products and apatite particles contributed to the mass loss of the composite scaffolds. The apatite particles were removed through centrifugation, and the mass loss of the matrix polymer after the hydrolytic degradation was evaluated in the current study. The degradation pattern was proposed for fibrous mats with different distributions of HA particles in the fiber matrix.

After being incubated into the degradation media, electrospun PDLLA fibrous mats floated, then suspended and immersed into the media. As shown in Fig. 6, non-woven mats changed from shrinking to swelling, meanwhile, the fiber size increased and the fiber space shrunk for PDLLA fibrous mats (Fig. 6a) and composites BEC (Fig. 6b), except for composites IGC (Fig. 6c). Fig. 6d shows a higher magnification of degradation site formed on the fiber surface with debonding of HA nanoparticles in composites IGC.

The molecular weight reduction and mass loss of electrospun PDLLA fibers, composites IGC and BEC with HA loading of 25.2% are summarized in Fig. 6e and f, respectively. It can be seen that the degradation rates of fibrous composites were higher than those of electrospun PDLLA fibers during the whole incubation process. It was indicated that the incorporation of HA into the PDLLA matrix was considered to slow down the degradation process by neutralizing or buffering the pH changes caused by the typical acidic degradation products of polyesters [6]. However, in the current study, the inoculation of HA did not slow down the degradation, and the surface wettability and microstructure of fibers should play great roles in the degradation process. Around 87.4 ± 3.2%, 44.7 ± 3.4% and 67.8 ± 3.2% of molecular weight residual and 77.6 ± 2.6%, 47.4 ± 4.4% and 72.3 ± 2.4% of mass residual for matrix polymers were detected after 10 wk incubation of electrospun PDLLA mats, fibrous composites BEC and IGC, respectively.

Different degradation patterns should exist between the pure PDLLA fibers and fibrous composites, resulting from their different surface wettability. During the electrospinning process, the high surface tension at the air/polymer interface, high-speed swing, the rapid solvent evaporation and solidification led to rough surface of electrospun fibrous mats, and the air entrapment between fibers interfaces resulted in hydrophobic fibrous surface [29]. It was also indicated that chemical groups with lower binding energy could be enriched on the fiber surface, resulting in the relative surface hydrophobicity of the electrospun PDLLA fibrous mat with WCA of 132.2 ± 1.5°. The high hydrophobicity and water repellent properties of electrospun PDLLA fibers led to slower water penetration into the fibrous mats, resulting in surface erosion pattern. SEM observations indicated significant conglutination for electrospun PDLLA fibers due to the degradation of matrix polymer, and the fiber size decreased due to the surface erosion and significant mass loss after incubation for 10 wk (Fig. 6a).

Fibrous composites IGC and BEC showed WCAs close to 0°, due to the enrichment of hydrophilic HA particles on the fiber surface. The water diffusion into the fibrous mats was enhanced, and the molecular chain started to break with the water diffusion into the fibers. The high surface area after the diffusion of HA particles out of the fibers of composites BEC led to significantly higher molecular weight reduction (Fig. 6e) and mass loss (Fig. 6f) than those of composites IGC and electrospun PDLLA fibers. The loosely interactions and the possible agglomeration of HA particles within the fiber matrices resulted in fiber breakage after removal of HA particles. As shown in Fig. 6b, there were stronger rupture and conglutination of the fibrous composite BEC compared to IGC. Although some particles debonded from fiber matrices and formed the degradation sites, most of HA particles interacted with PDLLA fibers and formed a shell around the fiber in composites IGC after 10 wk incubation (Fig. 6d). Therefore, the interactions between HA and the matrix polymer, the HA loading and distribution within the fibers showed effects on the degradation rate. Compared with the morphology before incubation (Fig. 1), the morphologies of electrospun fibers and the fibrous mats of composites IGC were more stable during the incubation due to the distribution of apatite phase

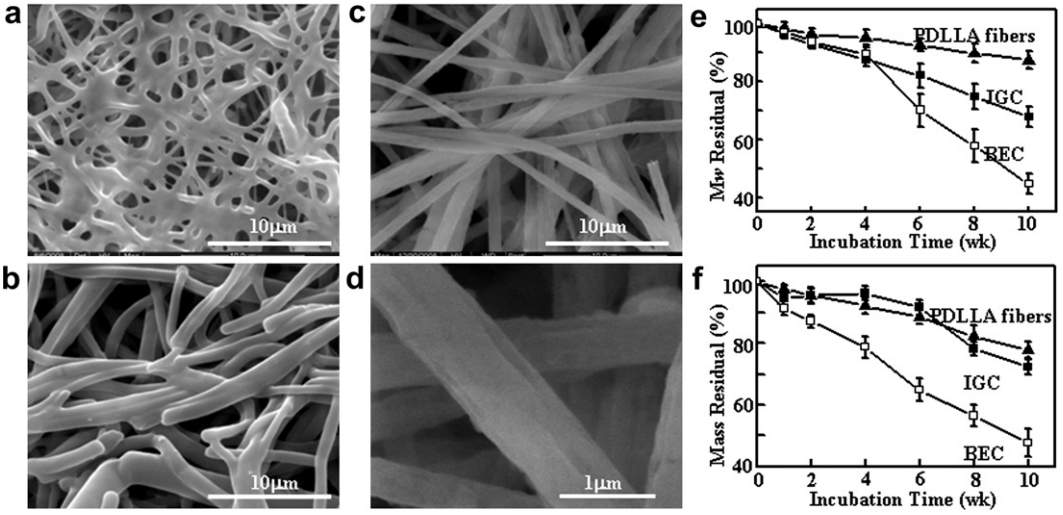

Fig. 6. SEM images of electrospun PDLLA fibers (a), HA/PDLLA fibrous composites from blend electrospinning (BEC, b) and *in situ* growth (IGC, c and d) with 25.2% of HA loadings after incubation in pH 7.4 PBS at 37 °C for 10 wk; Molecular weight reduction (e) and mass residual of matrix polymers (f) of electrospun PDLLA fibers, HA/PDLLA composites BEC and IGC after incubation in pH 7.4 PBS at 37 °C ($n = 3$).

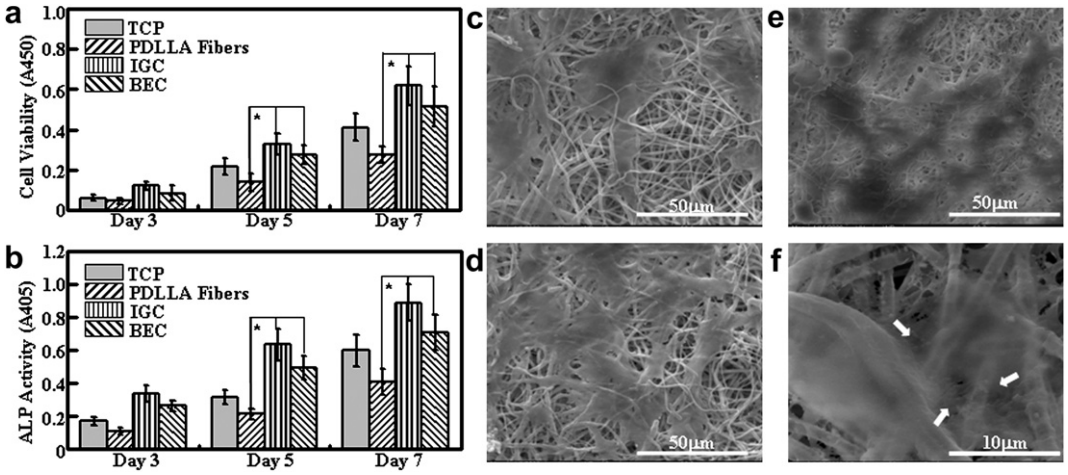

Fig. 7. The proliferation (a) and alkaline phosphatase activity (b) of MC3T3-E1 cells on tissue culture plates (TCP), electrospun PDLLA fibers, HA/PDLLA fibrous composites from blend electrospinning (BEC) and *in situ* growth (IGC) with 25.2% of HA loadings ($n = 3$, $^*p < 0.05$); SEM images of cells grown on electrospun PDLLA fibers (c), fibrous composites BEC (d) and IGC (e and f) after 7 d culture.

on the fiber surface, even when the degradation of matrix polymer was detected. The morphology stability was crucial for tissue engineering scaffolds to enhance the cell attachment and distribution into the whole scaffold.

3.6. Cell growth behaviors on fibrous composites

MC3T3-E1 cells were cultured on composites BEC and IGC with 25.2% of HA loadings and electrospun PDLLA fibers, and the cell behaviors were assessed on days 3, 5 and 7 after incubation. As shown in Fig. 7a, the cell proliferation increased significantly on days 5 and 7 on fibrous composites IGC and BEC compared to electrospun PDLLA mats and TCP ($p < 0.05$). The osteoblastic differentiation of MC3T3-E1 cells was investigated by the ALP activity. As shown in Fig. 7b, on days 5 and 7, the ALP activity levels were significantly higher on the composite mats than those on electrospun PDLLA fibers and TCP ($p < 0.05$). It was indicated that the degradation of ACP would release Ca and P ions into the surrounding environment, which was found to be responsible for the osteoconduction properties of ACP [30]. Therefore, the formation of ACP in the fibrous composite would render the composite bioactive. As shown in Fig. 7a and b, the cell viability and ALP activity levels on fibrous composites IGC were significantly higher than those of composites BEC ($p < 0.05$). The *in situ* growth of an apatite mineral phase on the fiber surface was considered to have the benefits of not only improving the surface hydrophilicity but also stimulating the osteogenic properties.

As shown in Fig. 7, the cells proliferation and osteogenic activity on the PDLLA fibrous mats were significantly lower than those on TCP ($p < 0.05$). Electrospun PDLLA fibers exhibited a hydrophobic surface with WCA of $132.2 \pm 1.5^\circ$ [29]. The adhesion and growth of cells on a surface were considered to be strongly influenced by the balance of hydrophilicity and hydrophobicity. Many studies have demonstrated that cells adhere, spread and grow more easily on moderately hydrophilic substrates than on hydrophobic or very hydrophilic ones [31]. Meanwhile, large dimensional changes (e.g. shrinkage) can occur in electrospun fibrous scaffolds of PDLLA [32], which may unfavorably chock the embedded cells in the scaffolds.

SEM morphologies of MC3T3-E1 cells grown on electrospun PDLLA mats, composites BEC and IGC are shown in Fig. 7c–e, respectively. Cells were observed spanning the gaps between electrospun fibers, as indicated by the flattened and spreading morphology covering the surface. A higher cell density was observed on the surface of fibrous composites IGC and BEC. After 7 d culture, the surface of the fibrous composite IGC was almost covered with cells and possibly mixed with the secreted extracellular matrix. As shown in Fig. 7f, cells on the composite IGC showed the extension of filopodia and anisotropic aggregation of a number of highly spread pre-osteoblasts with morphology that looked similar to viable osteoblasts. Meanwhile, it revealed normal cell morphology with the formation of mineral particles on the surface (Fig. 7f). These results suggest that the fibrous composite and the localization of apatite phase on the fiber surface act as an excellent cell support to maintain desirable cell–substrate interactions, to provide favorable conditions for cell proliferation and to stimulate the osteogenic differentiation.

4. Conclusions

Fibrous HA/PDLLA composites formed from *in situ* growth of HA within ultrafine fibers were investigated as potential tissue engineering scaffolds. The interactions between the matrix polymer and formed HA and the high HA loadings enhanced the mechanical performances and stable interfaces. The localization of apatite phase on the fiber surface of the composite IGC was demonstrated to improve the biomineralization ability after incubation into SBF, and to enhance the morphological stability of the fibers and fibrous mats during incubation into the degradation media. The non-stoichiometric HA particles existed on the fiber surface was able to maintain desirable cell–substrate interactions, provide favorable conditions for cell proliferation and stimulate to undergo osteogenic differentiation. *In situ* grown fibrous composites showed potentials as coating materials on medical devices and scaffolds for tissue regeneration.

Acknowledgments

This work was supported by National Natural Science Foundation of China (20774075 and 51073130), and National Key Project of Scientific and Technical Supporting Programs Funded by MSTC (2006BAI16B01).

References

[1] Rezwan K, Chen QZ, Blaker JJ, Boccaccini AR. Biomaterials 2006;27:3413–31.
[2] Agarwal S, Wendorff JH, Greiner A. Polymer 2008;49:5603–21.
[3] Kretlow JD, Mikos AG. Tissue Eng 2007;13:927–38.

[4] Deng XL, Sui G, Zhao ML, Chen GQ, Yang XP. J Biomater Sci Polym Ed 2007;18:117–30.
[5] Kim HW, Lee HH, Knowles JC. J Biomed Mater Res 2006;79A:643–9.
[6] Xu XL, Chen XS, Liu AX, Hong ZK, Jing XB. Eur Polym J 2007;43:3187–96.
[7] Hu X, Johnson RB, Schlea MR, Kaur J, Shofner ML. Polymer 2010;51:748–54.
[8] Venugopal J, Low S, Choon AT, Bharath KA, Ramakrishna S. J Biomed Mater Res 2008;85A:408–17.
[9] Chen J, Chu B, Hsiao B. J Biomed Mater Res 2006;79A:307–17.
[10] Cui WG, Li XH, Chen JG, Zhou SB, Weng J. Cryst Growth Des 2008;8:4576–82.
[11] Cui WG, Li XH, Xie CY, Zhuang HH, Zhou SB, Weng J. Biomaterials 2010;31:4620–9.
[12] Cui WG, Li XH, Zhou SB, Weng J. J Biomed Mater Res 2007;82A:831–41.
[13] Deng XM, Xiong CD, Cheng LM. J Polym Sci Part C 1990;28:411–6.
[14] Qi MB, Li XH, Yang Y, Zhou SB. Eur J Pharm Biopharm 2008;70:445–52.
[15] Cui WG, Li XH, Zhou SB, Weng J. J Appl Polym Sci 2007;103:3105–12.
[16] Wang CK, Ju CP, Chern Lin JH. Mater Chem Phys 1998;53:138–49.
[17] Ito Y, Hasuda H, Kamitakahara M, Ohtsuki C, Tanihara M, Kang IK, et al. J Biosci Bioeng 2005;100:43–9.
[18] Liao S, Xu GF, Wang W, Watari F, Cui FZ, Ramakrishna S, et al. Acta Biomater 2007;3:669–75.
[19] Sabokbar A, Millett PJ, Myer B, Rushton N. Bone Miner 1994;27:57–67.
[20] Furuichi K, Oaki Y, Imai H. Chem Mater 2006;18:229–34.
[21] Sato K, Kumagai Y, Tanaka J. J Biomed Mater Res 2000;50:16–20.
[22] Hsueh CH. J Am Ceram Soc 1987;72:344–7.
[23] Yang XM, Li L, Shang SM, Tao XM. Polymer 2010;51:3431–5.
[24] Zhou SB, Zheng XT, Yu XJ, Wang JX, Weng J, Li XH, et al. Chem Mater 2007;19:247–53.
[25] Suh H, Hwang YS, Lee JE, Han CD, Park JC. Biomaterials 2001;22:219–30.
[26] He QJ, Huang ZL. J Crystal Growth 2007;300:460–6.
[27] Kim HM, Himeno T, Kokubo T, Nakamura T. Biomaterials 2001;26:4366–73.
[28] Babensee JE, Anderson JM, McIntire LV, Mikos AG. Adv Drug Del Rev 1998;33:111–39.
[29] Cui WG, Li XH, Zhou SB, Weng J. Polym Degrad Stabil 2008;93:731–8.
[30] Shen WJ, Chung KC, Wang GJ, McLaughlin RE. J Arthroplasty 1992;7:43–9.
[31] Arima Y, Iwata H. Biomaterials 2007;28:3074–82.
[32] Cui WG, Zhu XL, Yang Y, Li XH, Jin Y. Mater Sci Eng C 2009;29:1869–76.